Available online at www.sciencedirect.com
SCIENCE DIRECT®
ELSEVIER
Marine Structures 16 (2003) 437–468
MARINE STRUCTURES
www.elsevier.com/locate/marstruc

Sensitivity analysis on ultimate strength of aluminium stiffened panels

P. Rigo[a,*], R. Sarghiuta[b], S. Estefen[c], E. Lehmann[d], S.C. Otelea[d], I. Pasqualino[c], B.C. Simonsen[e], Z. Wan[f], T. Yao[g]

[a] *ANAST, University of Liege (FNRS), Chemin des Chevreuils 1, 4000 Liège, Belgium*
[b] *Technical University of Civil Engineering of Bucharest, 124 Lacul Tei Bd. Sect 2, 72302 Bucharest, Romania*
[c] *COPPE, Universidade Federal do Rio de Janeiro, Caixa Postal 68510, Rio de Janeiro 21945-970, Brazil*
[d] *Technische Universität Hamburg-Harburg, Lämmersieth 90, 22305 Hamburg, Germany*
[e] *Technical University of Denmark, Dept. of Naval Architecture and Offshore Engineering, Building 101 E, DK-2800 Kgs. Lyngby, Denmark*
[f] *China Ship Scientific Research Center, P.O. Box 116, Wuxi 214082, China*
[g] *Naval Architecture and Ocean Engineering, Osaka University, 2-1 Yamada-Oka, Suita, Osaka 565-0871, Japan*

Received 24 February 2003; received in revised form 19 August 2003; accepted 4 September 2003

Abstract

This paper presents the results of an extensive sensitivity analysis carried out by the Committee III.1 "*Ultimate Strength*" of ISSC'2003 in the framework of a benchmark on the ultimate strength of aluminium stiffened panels.

Previously, different benchmarks were presented by ISSC committees on ultimate strength. The goal has typically been to give guidance to the designer on how to predict the ultimate strength and to indicate what level of accuracy would be expected.

This time, the target of this benchmark is to present reliable finite element models to study the behaviour of axially compressed stiffened aluminium panels (including extruded profiles). Main objectives are to compare codes/models and to perform quantitative sensitivity analysis of the ultimate strength of a welded aluminium panel on various parameters (typically the heat-affected zone).

Two phases were planned. In *Phase A*, all members analysed the same structure with a defined set of parameters and using different codes. It was expected that all the codes/models predict the same results. In *Phase B*, to boost the scope of the analysis, the different members

*Corresponding author. Tel.: +32-4-366-9366; fax: +32-4-366-9133.
E-mail address: ph.rigo@ulg.ac.be (P. Rigo).

doi:10.1016/j.marstruc.2003.09.002

(using their own model) performed FE analyses for a range of variation of different parameters (sensitivity analysis).

Keywords: Ultimate strength; Sensitivity analysis; Aluminium stiffened panels; Axial compression; Heat-affected zone

1. Introduction

Multi-stiffened aluminium panels are increasingly used in a variety of marine structures, with applications such as hull and decks in high-speed ferries and catamarans, and superstructures for ships. Other applications are box-girder bridges, walls and floors in offshore modules and containers. This development has primarily been driven by the demand for reduced structural weight, increased payload, and higher speed and reduced fuel consumption. The competitiveness of such structures is principally due to modern extrusion technology, new joining technologies such as friction stir welding and efficient manufacturing processes.

A relatively little experience has been accumulated from large aluminium structures, and the existing design recommendations for aluminium panels are often based on experience from steel structures. Therefore, the alloy-dependent material properties and the detrimental effects of welding are not always fully accounted for in codes. Often effects of improved tolerances, possibility of more efficient stiffener design and welding technology (as friction welding) are not adequately taken into account in the design recommendations.

Compared to steel panels, the ultimate strength of aluminium structures is sensitive not only to residual stresses and initial deformations, but to deterioration of mechanical strength in heat-affected zones (HAZ) also. During the thermal cycle of welding process, softening of the material readily creates a HAZ. The level of the strength decrease is dependent on alloy type, temper, welding process and welding parameters. The extent of the reduced strength zone is mainly depending on the welding process, the welding parameters and the material properties. Because of the good heat conductivity of aluminium, the HAZ is much wider than for steel (usually 20–25 mm).

The available literature on numerical analyses of the ultimate strength of stiffened aluminium plates is quite limited. Numerical analyses of aluminium panels have been carried out in several studies, using different approaches. The ultimate strength of stiffened aluminium AA6082-T6 plates under the axial compression was investigated by Aalberg et al. [1,2] using numerical and experimental methods. Kristensen and Moan [3] demonstrated numerically the effect of HAZ and residual stresses on the ultimate strength of rectangular aluminium plates (AA5083 and AA6082) under the bi-axial loading of plates. Some initial experimental and numerical simulations on torsional buckling of flatbars in aluminium panels have been also presented by Zha and Moan [4–6].

Hopperstad et al. [7] carried out a study with the objective of assessing the reliability of non-linear finite element analyses in predictions on ultimate strength of aluminium plates subjected to in-plane compression.

2. Reference panel description

2.1. Geometry

A three-spans panel with L-shaped stiffeners fabricated from extruded aluminium profiles in alloy AA6082 temper T6, joined by welding, was defined for the finite element analyses. The dimensions of the initial model are presented in Fig. 1 with the XYZ coordinate frame and the U, V, W corresponding displacements.

2.2. Loads

The behaviour of stiffened plates under compressive loads, which dominate the ship hull design, is relatively complex due to the large number of combinations of structural, material and loading parameters. In practice, the stiffened plates can be loaded in a variety of ways. In our analyses, only axial compressive loads are

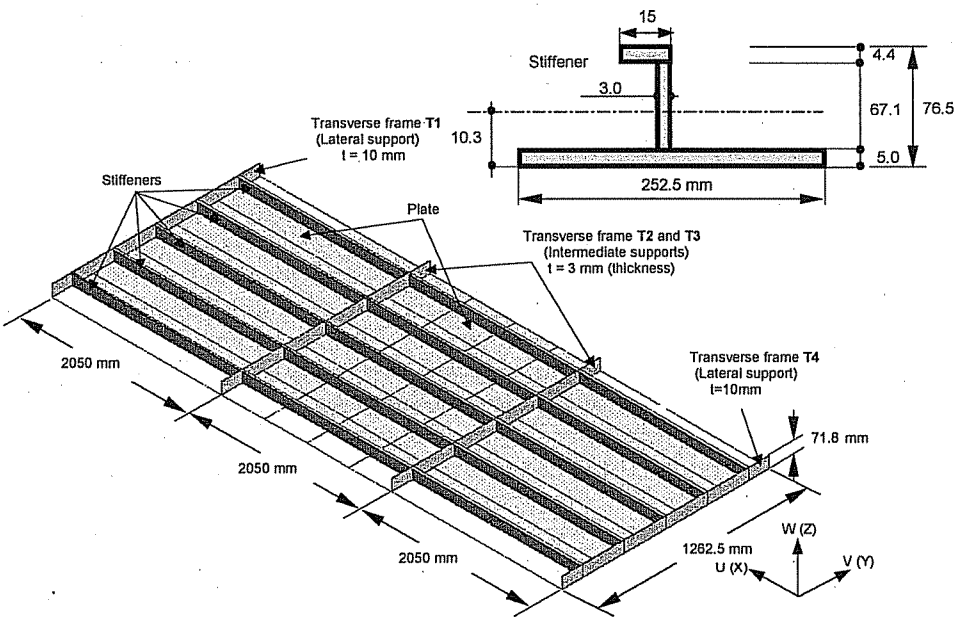

Fig. 1. The three-spans model (3 × 2050 mm) with a column slenderness (λ) of 1.80 (shortened in *Phase B* with 3 spans of 1025 mm and $\lambda = 0.90$).

applied at the initial neutral axis at both ends (no shift due to eccentric load, etc. is assumed). Lateral load, shear force, bi-axial in-plane stresses and in-plane bending stresses are not applied. Deadweight is not considered and a uniform temperature is assumed.

2.3. Material properties

The material is assumed isotropic with a Poisson's ratio of 0.3. The material properties (Fig. 2) were taken from the Aalberg experiments [1] and a Young Modulus of 70,475 N/mm^2 was found. The same material properties are considered for the four transverse frames.

The aluminium material strength in the HAZ is reduced by the high temperature during weld thermal cycle (MIG welded). The $\sigma - \varepsilon$ curve of the material inside the HAZ is also presented in Fig. 2.

True stresses versus true strain properties derived from engineering values were implemented by each user into his FE model for plate, stiffeners and HAZ.

Note: Hereafter T1,...,T4 will refer to the transverse frames and not to material temper.

2.4. Boundary conditions

The authors selected a three-spans FE model (instead of a standard $\frac{1}{2}+1+\frac{1}{2}$ model) with restrained rotation at the two ends (Fig. 1) as within the benchmark framework of the ISSC Committee the model and its boundary conditions were found clear and easy to implement with less risk of

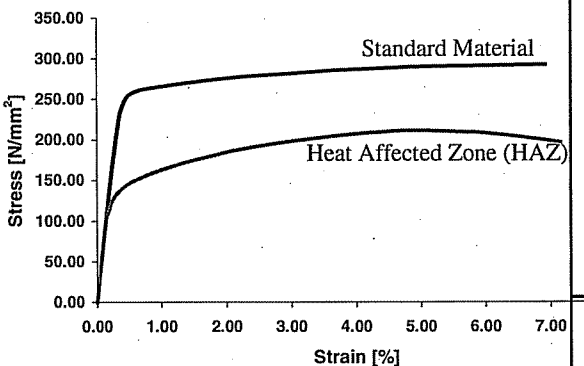

Plate and stiffeners			Heat Affected Zone		
N° Point	Strain [%]	Stress N/mm^2	N° Point	Strain [%]	Stress N/mm^2
1	0.00	0.0	1	0.00	0.0
2	0.21	146.3	2	0.14	100.0
3	0.34	222.6	3	0.19	113.7
4	0.36	232.4	4	0.24	124.8
5	0.39	240.1	5	0.33	136.0
6	0.43	247.1	6	0.48	145.2
7	0.47	253.3	7	0.71	154.1
8	0.54	257.3	8	1.02	163.4
9	0.65	260.6	9	1.36	171.9
10	0.80	263.0	10	1.70	178.5
11	1.33	269.4	11	2.12	186.6
12	2.18	276.9	12	2.70	194.6
13	3.10	282.2	13	3.37	201.7
14	3.75	285.5	14	3.99	206.9
15	4.74	288.9	15	4.41	209.3
16	5.27	290.0	16	4.79	211.2
17	6.92	292.2	17	5.24	210.7
			18	5.61	209.5
			19	5.96	208.1
			20	6.42	204.3
			21	6.84	200.3
			22	7.16	196.8

Fig. 2. Material curves (eng. stress) for the plate-stiffeners and for the HAZ [1].

misunderstanding. For the same reasons the standard procedure to establish the initial imperfection settings (performing buckling eigenvalue analysis) was not followed (see Section 2.5).

In the present FE computations, the boundary conditions for the stiffened panels were assumed simply supported along the two longitudinal edges (unloaded), which are kept straight (constrained edges).

The loaded edges were restrained from rotation and an axial displacement was prescribed ($W = V = 0$ and restrained rotation $W_x = 0$ with $U = 0$ on one side and $U = U^*$ on the other side). At these two loaded edges, the stiffener cross-section remains plane as the stiffened panel is supported by stiff transverse frames. The two end frames (T1 and T4) are assumed perfectly rigid-body (Fig. 1) and are modelled by thick transverse plates. Their dimensions are $1262.5 \times 71.8\,\text{mm}^2$ and thickness 10 mm.

At the intermediate support locations, transverse plates are also provided, T2 and T3 with thickness of 3 mm (Fig. 1). Then, the five longitudinal stiffeners are supported by the two intermediate and the two end plates (frames), the sideways deformation of the stiffeners being not allowed. In order to simulate stiff transverse frames, the displacements (W) along Z of these four transverse plates are not allowed. $W = 0$ is assumed for all the nodes at the intersection between the main plate and the four transverse support plates (Fig. 3).

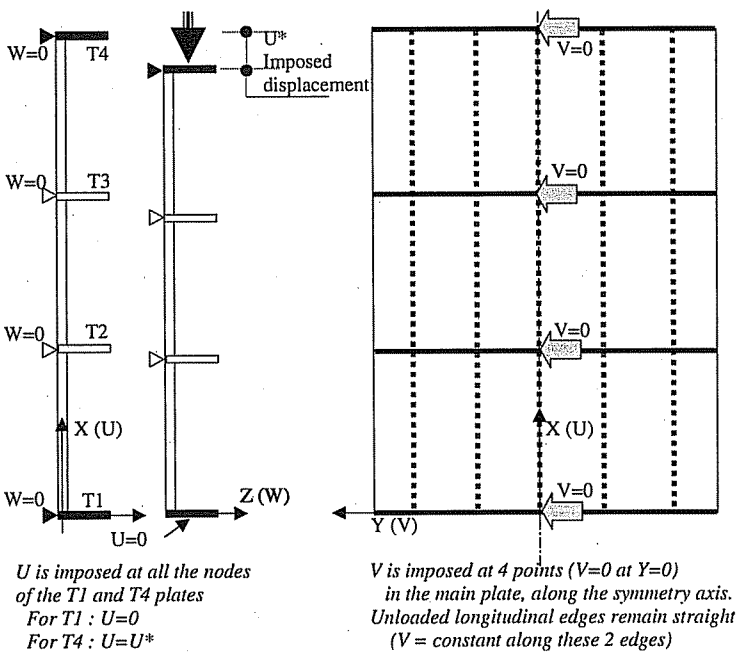

Fig. 3. Boundary conditions.

2.5. Initial imperfections

Plate and stiffener imperfections were considered using the following procedure (Fig. 4): a uniform lateral pressure is applied (on the opposite side of the stiffener—tip of stiffener in tension) on the overall structure (on the three-spans model). The pressure has to remain small to stay in the elastic range. The pressure was calibrated to obtain a linear elastic deflection (W) of 2 mm at the central point of the central panel, i.e. at mid-span of the central stiffener.

Shape and amplitude of the initial imperfections (for plates and stiffeners) are assumed identical to the deflections induced by the uniform lateral pressure. The displacements at each node were captured and used to define the initial configuration, i.e. the geometry of the FEM model. It is stated that these imperfections do not induce stresses.

Even if it is not a common procedure, this procedure has been selected to ease and simplify the modelling work of the participants. This initial deflection shape is of a thin-horse mode and is composed of several deflection components including the local buckling mode.

2.6. HAZ modelling

According to several standards, one shall consider the width of the reduced strength zone (noted η_1 and η_2 in the following) to extend 25 mm at each side of the weld (note that 20 mm is proposed in Eucode 9). In the present study (Fig. 5), this

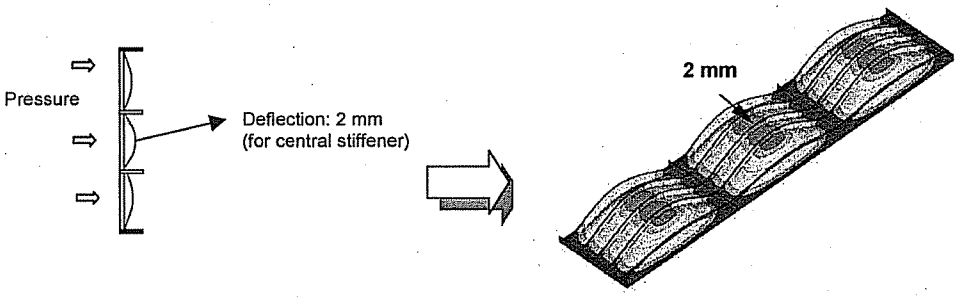

Fig. 4. Procedure to define the initial imperfections.

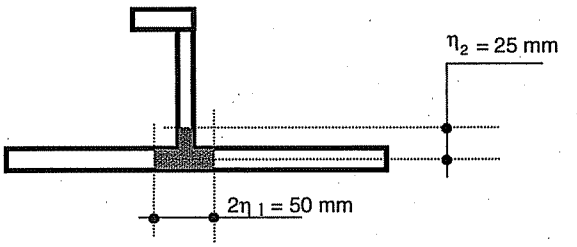

Fig. 5. Standard HAZ width ($2\eta_1$ in plate = 50 mm, η_2 in stiffener web = 25 mm).

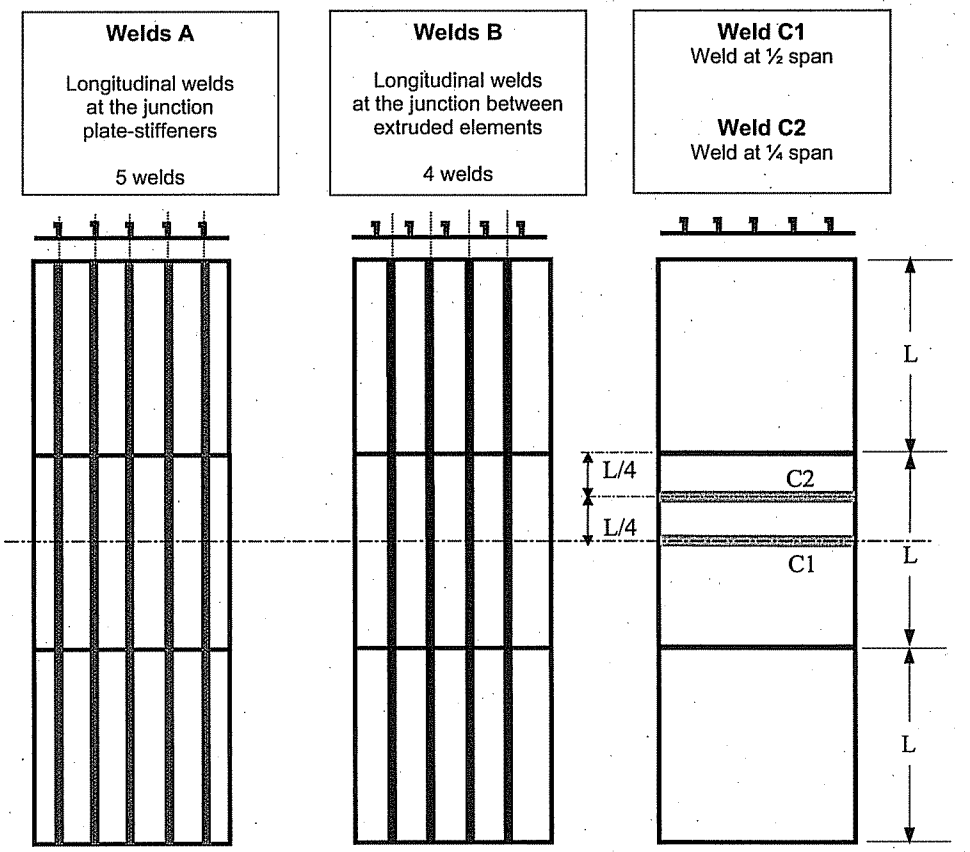

Fig. 6. Weld positions (HAZ width = 2 × 25 mm in plating and 25 mm in stiffener web plate measured from midplane of plate).

means $2\eta_1 = 50$ mm in the plate and $\eta_2 = 25$ mm in the stiffener web (measured from the mid-plate and not from the plate surface). The extension (width) of the HAZ is mainly affected by the applied welding process and the welding parameters, as well as the material properties. Therefore, the following weld zones were considered in the mesh model (Fig. 6):

- five longitudinal welds at the junction between the transverse plate and the five stiffeners,
- four longitudinal welds at the intersection between the five extruded elements,
- two transverse welds between plates.

It was assumed that the HAZ does not affect the transverse frames material (T1,...,T4).

If not specified, the numerical analyses were conducted with a HAZ width of 50 mm, i.e. $2\eta_1 = 50$ mm (2×25 mm in the plate) and $\eta_2 = 25$ mm in the stiffener flange, with η_1 and η_2 defined in Fig. 5.

3. Finite element modelling

Information concerning the codes and meshes used by the participants are presented in Table 1.

Lehmann–Catalin: The commercial FE code MSC Marc was used (Table 1). The system of non-linear equations is solved with the Newton–Raphson approach, in about 350 steps. Elasto-plastic formulation with piecewise linear workhardening is used for the material. The yield surface is von Mises, and the hardening law is isotropic.

Philippe–Radu: The stiffened plate panel was modelled using the commercial FE code ANSYS. The *Shell* 43 element was used to mesh the whole geometry. This four-node element has six degrees of freedom per node. An elasto-plastic model with von Mises yield criterion and multi-kinematic strain hardening was used to model the material constitutive behaviour. Axial compression was simulated by an imposed displacement in X direction, applied in small enough increments to ensure that the analysis would closely follow the structure's load–response curve. In order to help the problem to converge, optional program features as line search, automatic load stepping and bisection were activated.

Pasqualino–Estefen: The model was developed with the aid of the FE program ANSYS (*Shell* 43). The FEmesh was set in order to properly define the HAZ regions and keep good aspect ratio for the elements (Table 1). The mesh model of the L-stiffeners could be more refined but it would generate an extremely heavy model. The defined mesh comprises 10,320 elements, 10,453 nodes and 60,962 active degrees of freedom.

Yao–Higashiyama: ULSAS is a "*housemade*" code to model the collapse behaviour of structures considering the influence of material and geometrical non-linearities induced by yielding and large deflection. Both shell and beam-column elements are used in ULSAS (Table 1). For the shell element, an isoparametric shell element with four nodal points was used. They are degenerated elements with a linear displacement field and a reduced integration. An element of the same type with two nodal points was used as a beam-column element.

Wan: The FEA of stiffened plate with HAZ effects was completed by ANSYS (*Shell* 43) with about 20 different mesh sizes. The model includes 1866, 4242, 6042, 7150, 7842, 9642 and 12292 elements (Table 1). The multi-isotropic strain hardening law and von Mises yield criterion were applied in FEA.

Bo–Ulrik: The analysis was carried out using the explicit FE code LS-DYNA (Table 1). The material behaviour is modelled with a piecewise linear elastic–plastic model. The input to this model is true stress versus plastic true strain. The axial compression was simulated by an imposed displacement in the x-direction at the end of the stiffened panel.

Table 1
Software used by the contributors and meshing features

	FEM software	Mesh		Number of elements on a single line (or row)				
		Type of element	Total number of elements	Number of elements along X in one span of 1025 mm (or 2050 mm)	Number of elements along Y (between two stiff.)	Number of elements for the web (stiff)	Number of elements for the flange (stiff)	Number of elements on the plate HAZ's width
Lehmann–Catalin	MSC Marc	Shell	8520	40	8	3	1	2 for Weld A 2 for Weld B
Philippe–Radu—standard mesh	ANSYS	Shell43	6588	16	13	4	2	5 for Weld A 4 for Weld B
Philippe–Radu—Fine mesh	ANSYS	Shell43	13656	42	13	4	2	5 for Weld A 4 For Weld B
Pasqualino–Estefen	ANSYS	Shell43	10320	40	12	3	1	4 for Weld A
Wan (coarse mesh)	ANSYS	Shell143	1866	10	6	3	1	2 for Weld A
Wan (standard mesh)	ANSYS	Shell143	7150	36	6	5	1	2 for Weld A
Wan (fine mesh)	ANSYS	Shell143	12292	50	10	5	1	4 for Weld A
Yao—phase A (coarse mesh, M2)	ULSAS	Shell/beam	4160/480	96	20	4	Beam-column element	No
Yao—phase A (fine mesh, M4)	ULSAS	Shell/beam	14400/960	192	40	6	Beam-column element	No
Yao—phase B (final mesh)	ULSAS	Shell/beam	8880/480	96	50	6	Beam-column element	2 for Weld A 2 for Weld B
Bo–Ulrik	LS-DYNA	Shell	7850	32	13	4	2	5 for Weld A 4 for Weld B

4. Finite element analyses

The aim of *Phase A* was intended as a calibration assessment. This phase was divided in two steps: *Phase A*1 without effect of the HAZ and *Phase A*2 with the effect of the HAZ. The effect of residual stresses was not considered in *Phase A*. During that phase, all the contributors solved the same problem to validate their FE model and analysis procedure.

Then, for *Phase B*, the committee selected a series of parameters for the sensitivity analyses and each contributor performed different analysis. These parameters are:

- Weld types (longitudinal, transversal, extruded and no extruded components). Several configurations are studied—*Phase B*1,
- HAZ width ($2\eta_1 = 25-100$ mm)—*Phase B*2,
- Initial panel deflection (amplitude and shape)—*Phase B*3,
- Residual stresses—*Phase B*4,
- Plate thickness—*Phase B*5,
- Yield stress in the HAZ—*Phase B*6.

First, a model of three spans of 2050 mm was analysed by the contributors (*Phase A*) and it was found that the model is not sensitive to HAZ. Subsequently, a second model with three spans of 1025 mm was studied (*Phase B*).

4.1. Phase A1—calibration without HAZ

The results of the *Phase A*1 analyses (Fig. 7) are typical loading capacity curves provided by the different contributors. They are expressed in terms of "average strain–average stress" (also called stress–strain curve). The "average strain" is the ratio of displacement from the loading capacity curve to the length of the panel, and the "average stress" is the force given by the loading capacity curve divided by the

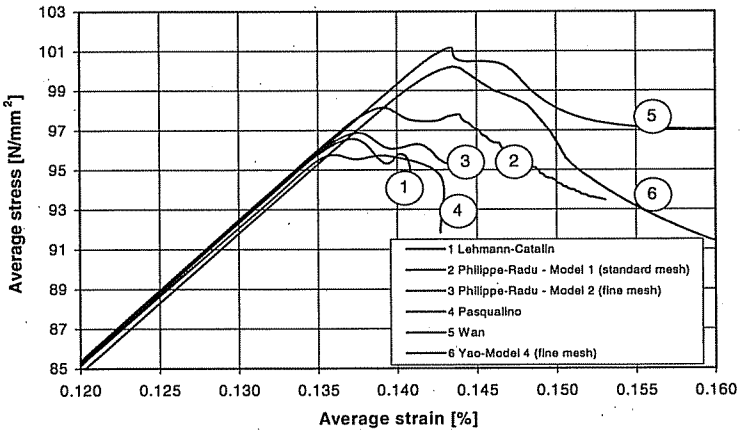

Fig. 7. Results of comparison at *Phase A*1 (3 × 2050 mm spans model, without HAZ).

cross-sectional area of the panel. The model includes initial deflections (plate and stiffeners) and non-linear material properties.

The stress–strain curves obtained by the various contributors (Fig. 7) are almost similar. There is about 4% difference between the minimum and maximum values. These differences are probably induced by the size of the mesh models, the element types, the codes and the numerical procedures (number of steps, etc.) used by the contributors (Table 1).

4.2. *Phase A2—calibration with HAZ*

The following configurations were considered (Fig. 6): (1) Welds A; (2) Welds B; (3) Welds B + Weld C1; (4): Welds B + Weld C2 and (5) Welds A + Weld C2; where:

- Welds A are situated at the five junctions between the plate and the stiffeners,
- Welds B are situated at the four junctions between extruded elements,
- Weld C1 is situated at L/2 of the central span,
- Weld C2 is situated at L/4 of the central span.

For *Phase A*, the contributor results shown in Figs. 8a–d are summarised in Table 2. These figures show clearly that there are no significant differences between the contributors. For a given weld type, the stress–strain curve and the ultimate load of the different models are quite similar. All the models show a global flexural buckling collapse mode (Fig. 9, *bottom right*), with the middle field with displacements in negative direction, and the other two fields in positive direction (positive direction = the direction of the stiffeners). The first drop in the average stress/average strain curve corresponds to development of the flexural buckling, while the second drop corresponds to the stiffener tripping in the middle of the model.

Since the ultimate strength obtained through the simulations (about 100 N/mm^2, Fig. 2) does not reach the yield stress of the HAZ material (about 130 N/mm^2), we conclude that there is no HAZ effect for the considered panel. *Phase A* hence shows that the behaviour of the panel stays elastic until the collapse. It was therefore not possible with *Phase A* model to get any information about the influence of the HAZ material properties on the ultimate strength. So, for *Phase B*, the model geometry (and its associated column slenderness) was modified to have smaller spans, smaller column slenderness ($\lambda = 0.90$ instead of 1.80 for, respectively, 1025 and 2050 mm model span, Fig. 9) and therefore a higher ultimate strength (140–170 N/mm^2 instead of 100 N/mm^2). The column slenderness corresponds to the square root of the plastic squash load to the elastic buckling load and has usually a direct effect on the ultimate load of the panel (even if the model is not a column).

4.3. *Phase B1—weld types*

At the end of *Phase A* (Table 2), the committee was confident about the quality of their FE models and decided to start the next phase (*Phase B*). Each contributor was

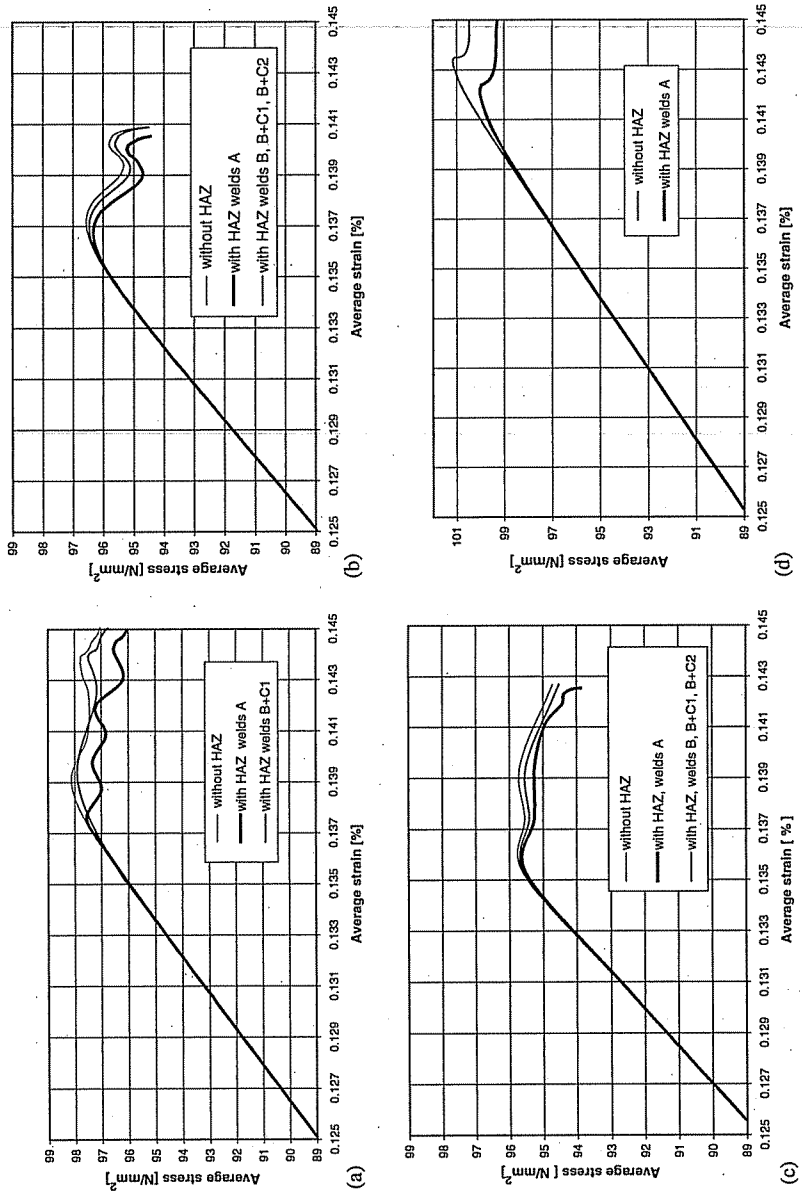

Fig. 8. (a) Effect of the HAZ on the initial model—3 × 2050 mm spans (*Phase A2*: Philippe–Radu's model); (b) effect of the HAZ on the initial model—3 × 2050 mm spans (*Phase A2*: Lehmann–Catalin's model); (c) effect of the HAZ on the initial model—3 × 2050 mm spans (*Phase A2*: Estefen–Pasqualino's model); and (d) effect of the HAZ on the initial model—3 × 2050 mm spans (*Phase A2*: Wan's model, standard mesh).

Table 2
Results of phase A1 and phase A2—3 × 2050 mm spans model

	Lehmann–Catalin			Philippe–Radu			Wan			Estefen–Pasqualino		
	Maximum average stress		Average strain (%)	Maximum average stress		Average strain (%)	Maximum average stress		Average strain (%)	Maximum average stress		Average strain (%)
	(N/mm^2)	Difference to reference		(N/mm^2)	Difference to reference (%)		(N/mm^2)	Difference to reference (%)		(N/mm^2)	Difference to reference (%)	
Without HAZ (reference)	96.57	Ref. (%)	0.1372	98.14	Ref.	0.1392	100.49	Ref.	0.1452	95.61	Ref.	0.1353
With HAZ												
Welds A	96.33	−0.25	0.1367	97.34	−0.82	0.1398	100.02	−0.46	0.1421	95.52	−0.10	0.1353
Welds B	96.47	−0.10	0.1369							95.57	−0.05	0.1353
Welds B+C1	96.47	−0.10	0.1369	97.91	−0.23	0.1392				95.57	−0.05	0.1353
Welds B+C2	96.47	−0.10	0.1369							95.57	−0.05	0.1353
Mean value	96.43	−0.14	0.137	97.62		0.139	100.02		0.142	95.55		0.135

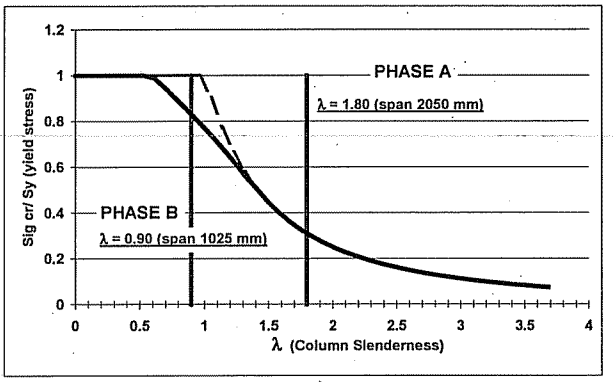

Phase A: failure induced by global flexural buckling followed by local tripping

Phase B: failure induced by stiffener tripping in the 2 end spans followed by a global flexural buckling of the central span.

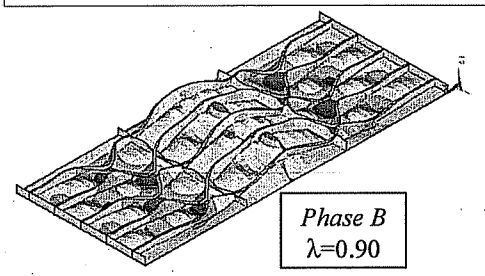

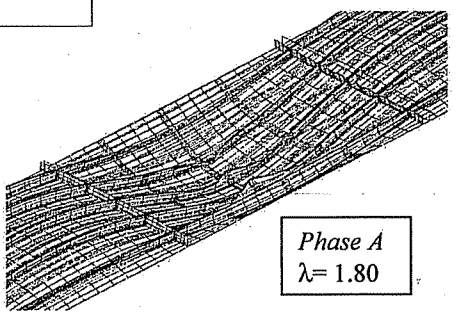

Fig. 9. Top: variation of the ultimate strength with the span (1025 and 2050 mm): *Bottom left*: Collapse mode at the ultimate strength stage (3 × 1025 mm model and $\lambda = 0.90$); and bottom right: Collapse mode at the ultimate strength stage (3 × 2050 mm model and $\lambda = 1.80$).

assigned to perform new analyses to assess the sensitivity of one or two parameters (*Phases B*1–*B*6).

For *Phase B*, a modified model was proposed to assess the effect of the HAZ on the ultimate strength. A new panel with three spans of 1025 mm was obtained by halving the span length of the initial model. The column slenderness (λ) of the new model became 0.90 instead of 1.80 for the 3 × 2050 mm model used in *Phase A*. The rest of the model remained the same as defined in *Phase A*. The geometric imperfections were determined using the same way.

An additional analysis without HAZ was performed to serve as a reference case. The differences between the collapse modes and associated ultimate strength of the different configurations are presented in Figs. 10a–c and Table 3. First, the plates located between two stiffeners and two frames buckle. Later stiffener tripping in the two extreme spans occurs and induces a global flexural buckling mode in the central span (Fig. 9, *bottom left*).

4.3.1. Weld types (sensitivity assessment) (Table 3)

- In general, effect of weld types and weld location vary from 0% (*Phase A*) to 30% (*Phase B1*, Fig. 10).

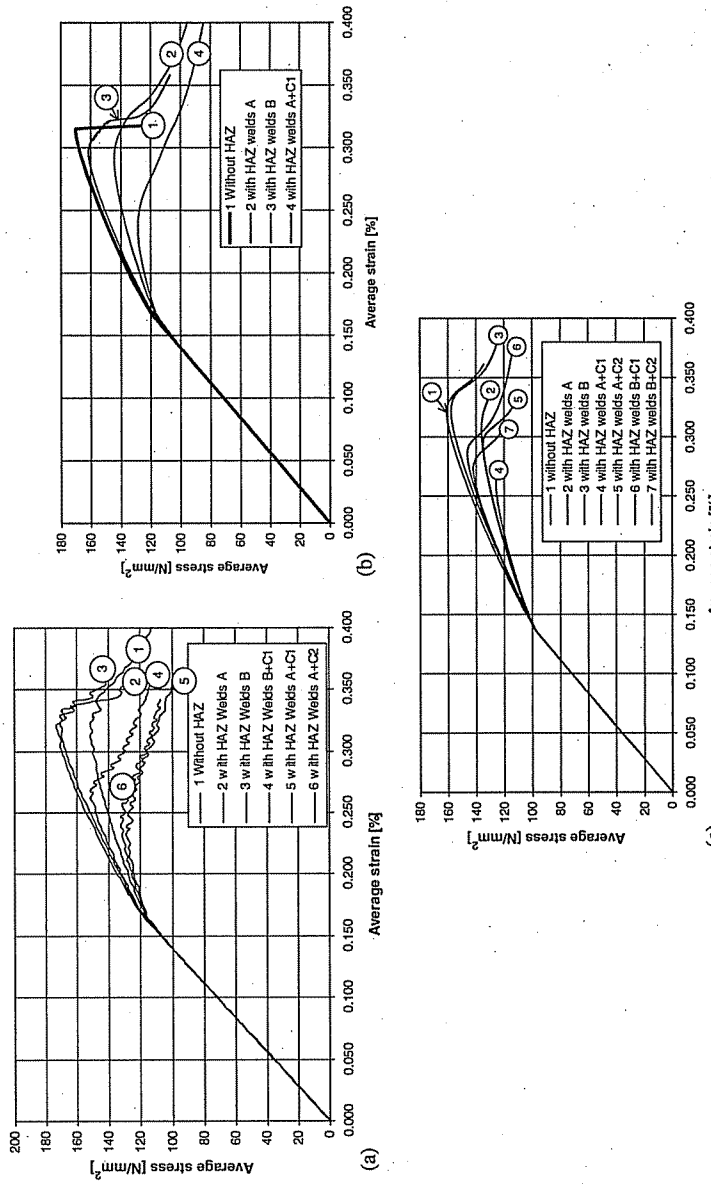

Fig. 10. (a) Effect of the HAZ on the new model—3 × 1025 mm spans (*Phase B1*: Philippe–Radu's model); (b) effect of the HAZ on the new model—3 × 1025 mm spans (*Phase B1*: Lehmann–Catalin's model); and (c) effect of the HAZ on the new model—3 × 1025 mm spans (*Phase B1*: Yao–Higashiyama's model).

Table 3
Phase B1: effect of the HAZ on the new model—3 × 1025 mm spans model

	Philippe–Radu (shape 2[a])			Lehmann–Catalin (Shape 1)			Yao–Higashiyama (Shape 1)		
	Maximum average stress		Average strain (%)	Maximum average stress		Average strain (%)	Maximum average stress		Average strain (%)
	(N/mm^2)	Difference to reference (%)		(N/mm^2)	Difference to reference (%)		(N/mm^2)	Difference to reference (%)	
Without HAZ (reference)	173.46	Ref.	0.321	169.88	Ref.	0.031	160.80	Ref.	0.300
	171.92 (if shape 1)								
With HAZ									
With HAZ Welds A	150.22	−13.40	0.300	144.48	−16.71	0.292	136.15	−21.51	0.301
With HAZ Welds B	171.21	−1.30	0.324	161.47	−6.91	0.296	157.70	−9.09	0.302
With HAZ Welds B+C1	151.61	−12.60	0.269	141.94	−18.17	0.246	146.28	−15.67	0.230
With HAZ Welds A+C1	129.12	−25.56	0.232	125.81	−27.47	0.259	126.10	−27.30	0.245
With HAZ Welds A+C2	132.93	−23.37	0.241	132.25	−23.76	0.244	135.09	−22.12	0.240
With HAZ Welds B+C2							142.05	−18.11	0.239
Mean value	147.02	−15.24	0.273	141.19	−18.60	0.267	140.56	−18.97	0.259

[a] Shape 2 was used by Philippe–Radu and Shape 1 by the other contributors. This may explain the difference, namely for analysis with Welds B.

- Longitudinal Welds B (panel with extruded elements): Effect of the HAZ is small (about 1–6%).
- Longitudinal Welds A (panel with welded stiffeners): Effect of the HAZ is larger and reaches 13–17%.
- Transverse Weld C1 and Weld C2: Effect of a single C1/C2 weld is about 7–12%. The weld location seems not very significant but cannot be neglected as a difference of 2–4% is recorded between Weld C1 and Weld C2. So, a transverse weld at mid-span should be avoided.
- Combined welds (A+C, B+C): When there are several weld types in the same simulation, it seems to be possible to add the individual effect of each weld type to estimate the total reduction. For instance, for a panel with Welds A+C1, the reduction is about 25–27% (15% for Welds A+11% for Weld C1).

4.4. *Phase B2–HAZ width (with Welds A—welded stiffeners)*

In *Phase B2*, the sensitivity analysis concerns the HAZ width (simulations with Welds A). Four HAZ widths ($2\eta_1$ in plate and η_2 in web) were considered (Fig. 5): $2\eta_1 = 25, 50, 75, 100$ mm ($\eta_2 = \eta_1$). Figs. 11 and 12, and Table 4 show the results of these analyses, which are compared to the reference case (without HAZ).

The variation of ultimate strength is not proportional to the HAZ width ($2\eta_1$). The first 25 mm of the HAZ width are the most significant and have the larger effect on the ultimate strength.

For the considered model with Welds A, we observed (Fig. 12 and Table 4):

- for $2\eta_1 = 25$ mm, the reduction is approximately 9%,
- for $2\eta_1 = 50$ and 75 mm, the additional reduction of ultimate strength is about 4.5%,
- for $2\eta_1 = 100$ mm, the additional reduction of ultimate strength becomes smaller, approximately 3.0%.

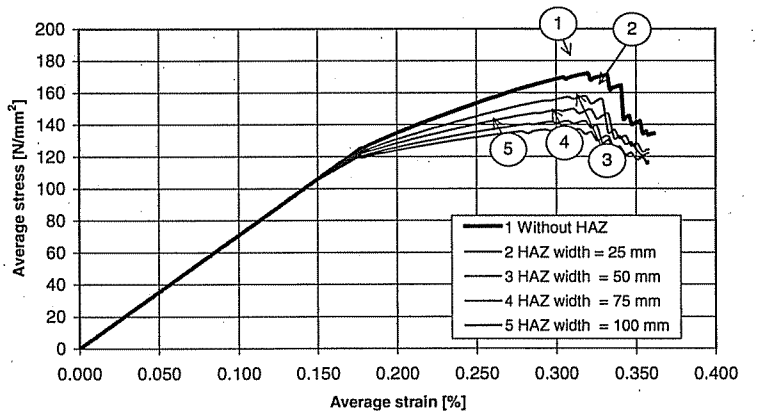

Fig. 11. Sensitivity on the HAZ width ($2\eta_1 = 25-100$ mm) (*Phase B2*: Philipe–Radu's model, 3×1025 mm, Welds A).

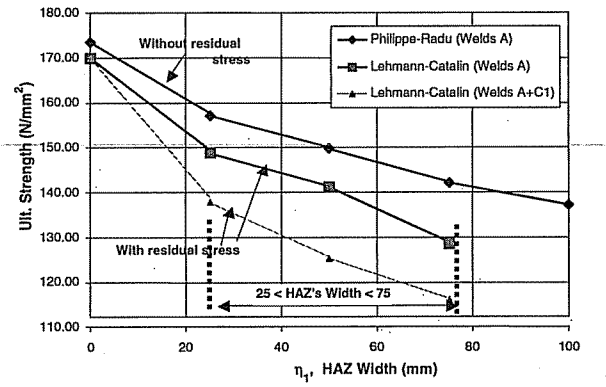

Fig. 12. Sensitivity on the HAZ width (*Phase B2*: Welds A and A+C1, $2\eta_1 = 25-100$ mm).

Table 4
Phase B2: sensitivity of the HAZ width—Welds A, 3 × 1025 mm spans model

(Init. deform: shape 1)	Maximum average stress		Average strain (%)
	(N/mm^2)	Difference to reference (%)	
(A) Phase B2 (Sensitivity on the HAZ width—25, 50, 75 and 100 mm) (without residual stress) Philippe–Radu			
Without HAZ (reference)	171.92	Ref.	0.320
With HAZ (Welds A)			
HAZ width = 25 mm	157.17	−8.58	0.308
HAZ width = 50 mm	149.75	−12.89	0.311
HAZ width = 75 mm	142.28	−17.24	0.308
HAZ width = 100 mm	136.96	−20.33	0.315
(B) Phase B2 (Sensitivity on the HAZ width—25, 50 and 75 mm) (with residual stress) Lehmann–Catalin			
Without HAZ (reference)	169.88	Ref.	0.312
With HAZ (Welds A)			
HAZ width = 25 mm	148.81	−12.41	0.274
HAZ width = 50 mm	141.20	−16.88	0.280
HAZ width = 75 mm	128.55	−24.33	0.279
With HAZ (Welds A + Weld C1)			
HAZ width = 25 mm	137.75	−18.92	0.245
HAZ width = 50 mm	125.42	−26.17	0.228
HAZ width = 75 mm	116.04	−31.69	0.214

Similar behaviour is recorded when residual stress is added (Table 4). With residual stresses in the model, the effect of the first 25 mm HAZ is even slightly bigger (12% instead of 9%).

For Welds A+C1 (with residual stress), the reductions are 19%, 7% and 5% instead of 12%, 4.5% and 7% (Table 4).

4.5. Phase B3—initial imperfection

The influence of the amplitude and shape of initial imperfection was studied in this phase (without HAZ). The amplitude is considered at the reference point, which is in the centre of the panel (Fig. 4). This deflection may be different from the panel's maximum deflection (Fig. 13), as significant local plate deflection may occur.

4.5.1. Shape effect (sensitivity assessment)

Two shapes of initial deflection were considered in the analyses. The first one, shape 1, was obtained by applying a uniform pressure on the new model (see Section 2.5). Shape 2 was captured from the *Phase* A model by halving procedure.

Even if the two shapes differ, the corresponding stress–strain curves are quite similar (Fig. 13 and Table 5). It is concluded that other shapes have further to be considered to accurately assess this parameter.

Fig. 14 gives the deflection history of the reference point of two adjacent plates. Due to the initial deflection shape (Fig. 13), the deflections at the two points are initially identical. When the axial compressive load is applied, the two plates buckle but in opposite direction. This failure process is confirmed by Fig. 14. As the initial deflection shape differs completely from the shape of the collapse mode, it induces a strengthening of the structure. In the considered case, a snap-through behaviour occurs.

4.5.2. Amplitude effect (sensitivity assessment)

Fig. 15 shows the results for different amplitudes of initial deflection corresponding to Shape 2. Sensitivity assessment is obtained from Fig. 16. On average, for the concerned model, each millimetre of initial deflection induces about 1.1% of reduction of the ultimate strength. Such a small variation shows that the amplitude of the initial deflection is not a key factor (for the considered panel).

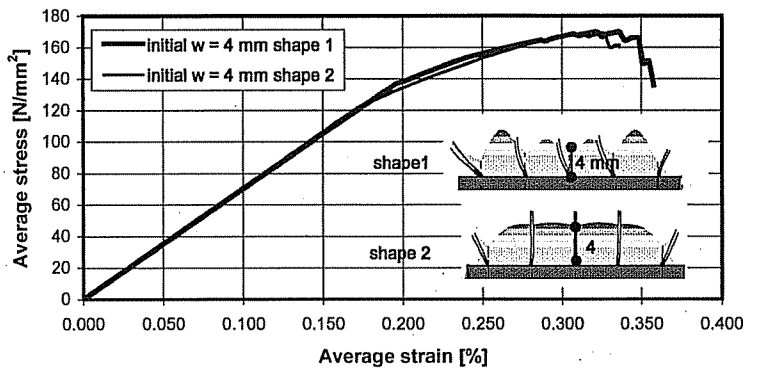

Fig. 13. Influence of the initial imperfections shape (*Phase B*3, 3 × 1025 mm model).

Table 5
Phase B3: sensitivity on initial deflection and shape Welds A, 3 × 1025 mm spans model, without HAZ

	Maximum average stress		Average strain (%)
	(N/mm^2)	Difference to reference (4 mm—shape 2) (%)	
Sensitivity of the deflection amplitude (2, 4 and 8 mm)—shape 2			
Initial deflection $w = 2$ mm—shape 2	173.46	+2.70	0.321
Initial deflection $w = 4$ mm—shape 2	168.89	Ref.	0.313
Initial deflection $w = 8$ mm—shape 2	162.11	−4.02	0.317
Sensitivity of the deflection shape (amplitude = 4 mm at the reference point—centre of the panel)			
Initial deflection $w = 4$ mm—shape1	169.71	+0.49	0.322
Initial deflection $w = 4$ mm—shape2	168.89	Ref.	0.313

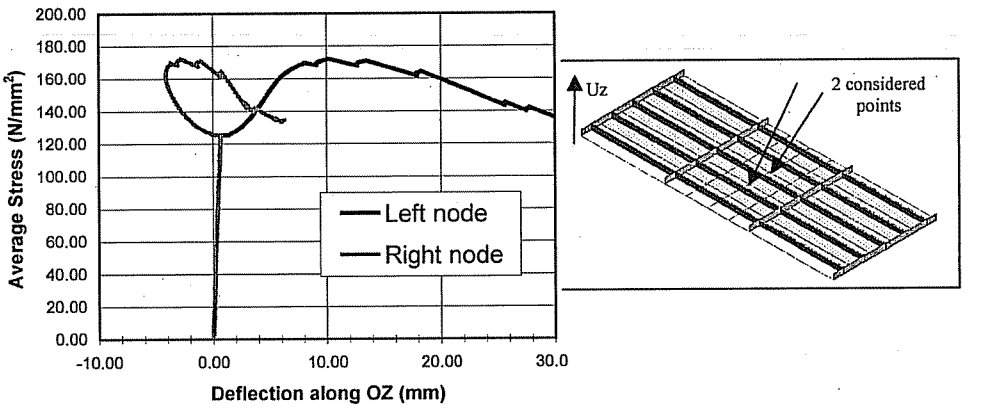

Fig. 14. Shape of the plate collapse mode (3 × 1025 mm model, without HAZ). Stress–deflection curves at the centre of two consecutive plates.

4.6. Phase B4—residual stresses

In this phase, *Lehmann–Catalin* have analysed the effect of the residual stresses in the HAZ on the ultimate strength of the panel. The distribution of the welding residual stresses based on the Zha and Moan paper [5] is presented in Fig. 17. Checking the effect of welding is, of course, a very difficult task. The simulation of welding itself is beyond the scope of work of this Committee. However, a simplified distribution of residual stresses was assumed (Fig. 17).

The initial stress pattern shown in Fig. 17 was implemented in the FE model as initial stresses. It is assumed that the initial tensile stresses extend over the entire HAZ width and are uniform over the width ($2\eta_1$) and through the plate thickness. Their direction is parallel to the welding seam and the magnitude is equal to the flow

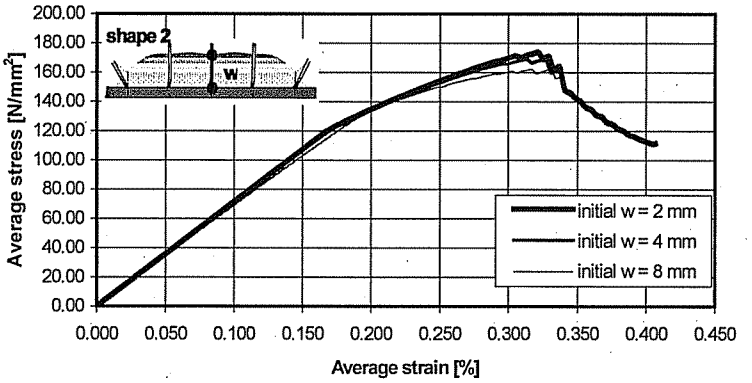

Fig. 15. Influence of the amplitude of initial imperfection (with shape 2) (*Phase B*3, 3 × 1025 mm spans model).

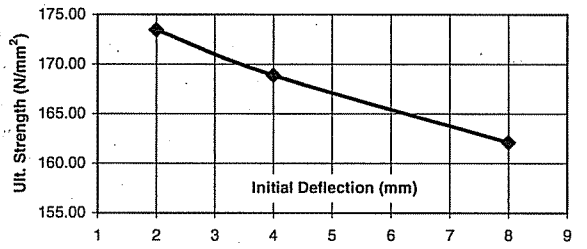

Fig. 16. Effect of the amplitude of the initial deflection (with shape 2) (*Phase B*3, 3 × 1025 mm spans model).

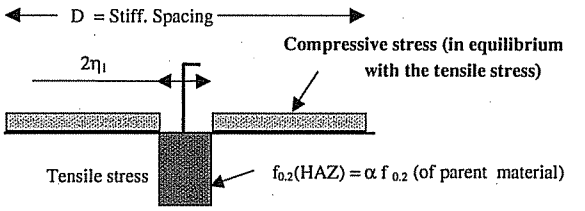

Fig. 17. Residual stress across the HAZ.

limit of the material of the HAZ, i.e. 130 N/mm^2 (Fig. 2). This is valid for the stresses in the plate, as well as for the stresses in the stiffener. If not specified, the standard HAZ width ($2\eta_1$) is 50 mm in the plate and 25 mm into the webs (η_2).

For the transversal welds, the residual stresses are acting perpendicular to the residual stresses of the longitudinal welding seams. The width of the field of compressive stresses in the plate is a problem, as it cannot be the entire length of the three-spans model. Therefore, they are considered to act only in the middle span of the model (1025 mm), between the two transversal beams (T2 and T3). The magnitude of the transversal residual stresses is determined in the same way as for the longitudinal ones.

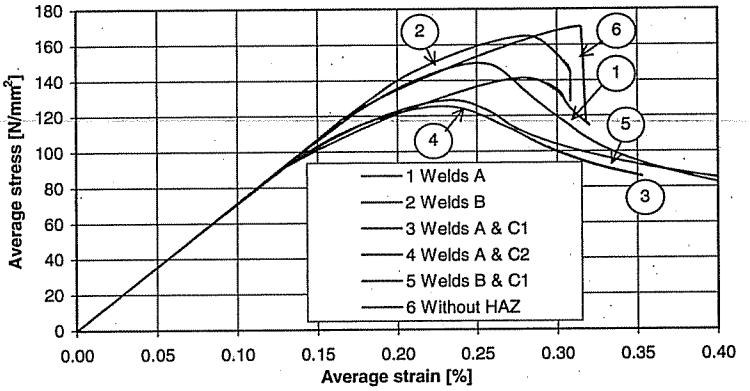

Fig. 18. Effects of weld types with residual stresses (*Phase B4*, 3 × 1025 mm spans model).

4.6.1. Weld positions and weld types (sensitivity assessment)

Similarly, as *Phase B1*, this effect is studied by a combination of longitudinal and transversal welding welds. The results are presented in Fig. 18 and Table 4. The tendency is the one already expected: the panel has a higher ultimate strength for Welds B (extruded element) than for welds A (stiffeners welded on the plate).

The same trend is obtained with or without residual stresses (compare Figs. 10 and 18, and Table 4). Ultimate strength reduction is a little bit larger with residual stress than without (excepted for Welds B).

It is interesting to take a close look at the ultimate stress curves for Welds B shown in Fig. 19, with residual stresses and without residual stresses. Both of them have the same HAZ material properties. It is surprising to see that the simulations with residual stresses provide higher ultimate strength. A feasible explanation for that phenomenon is that a tensile stress strip in the middle of a plate field is improving the buckling behaviour of the field. The buckling is triggered by the continuously increased lateral deflections that for many cases are maximum in the middle of the plate field. Therefore, we might conclude that the deflections in the middle strip have a great effect on buckling. If the residual tensile stresses in that strip are reducing the lateral deflections, it means that they improve the ultimate strength.

For Welds A, the opposite phenomenon takes place: the tensile stresses are localised at the boundary of the plate and the compressive stresses in the middle, resulting in a weaker panel.

4.6.2. HAZ width (sensitivity assessment)

Effect of the HAZ width combined with residual stresses was also assessed (Table 4). The width of the HAZ is modified and it becomes, respectively, $2\eta_1 = 25$, 50 and 75 mm for the plate, $\eta_2 = 12.5$, 25 and 37.5 mm for the stiffener (see also Table 4 for sensitivity to HAZ width without residual stresses). Fig. 20 shows the results for the configuration with Welds A (between the stiffeners and the plate) and Fig. 21 presents the results for Welds A + Weld C1.

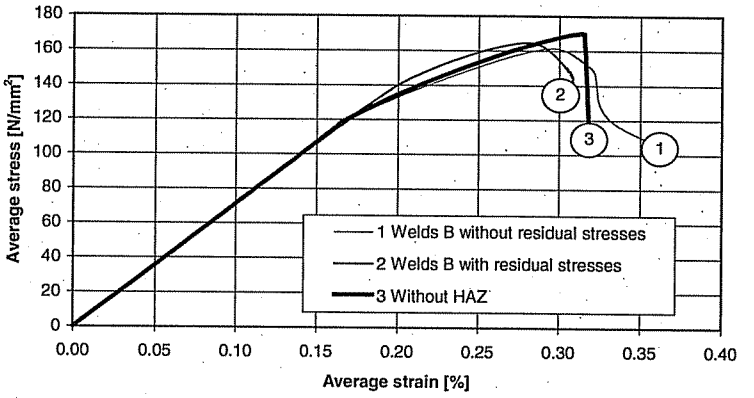

Fig. 19. Behaviour of Welds B with and without residual stresses (*Phase* B4, 3 × 1025 mm spans model).

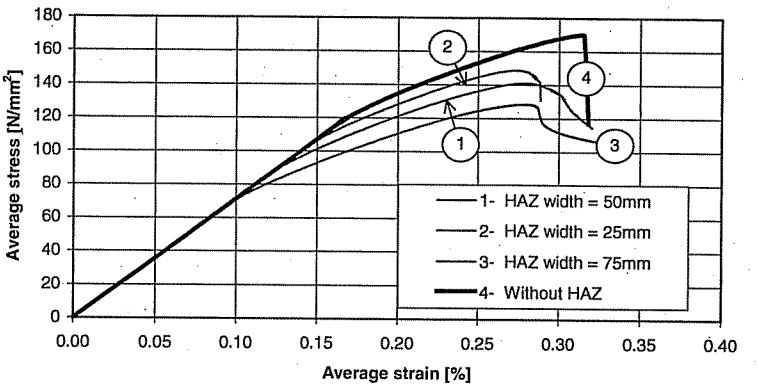

Fig. 20. Influence of the HAZ width ($2\eta_1$) (Welds A, with residual stresses, *Phase B4*).

4.6.3. Residual stresses (sensitivity assessment)

The ultimate average stress and corresponding average strain for each studied case are presented in Table 6. For the six cases, Fig. 22 compares the ultimate strength *with* and *without* residual stresses. Comparing the two categories, it can be noted the same trends with slightly smaller ultimate strength in the case *with residual stresses*.

Sensitivity assessment is obtained from Table 6 and Fig. 22. On average, the ultimate strength is reduced by 2.5% for plate 5 mm thick and 5% for 7 mm thick. These rates are just indicative as they can vary drastically (i.e. with Welds B).

4.7. Phase B5—plate thickness

Two additional analyses were done to check the coupled effect of the plate thickness and the welding residual stresses. The thickness of the plate was increased

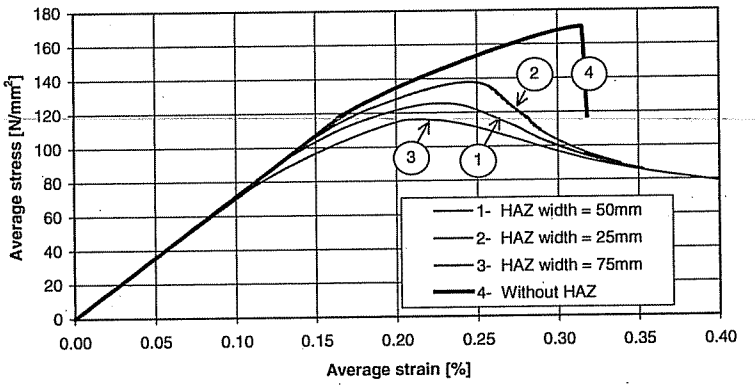

Fig. 21. Influence of the HAZ width ($2\eta_1$) (Welds A and C1, with residual stresses, *Phase B4*).

Table 6
Phase B4: sensitivity to residual stresses—3 × 1025 mm spans model

	Maximum average stress		Average strain (%)
	(N/mm^2)	Difference to reference (%)	
Plate of 5 mm			
Without HAZ	169.88		0.312
With HAZ (HAZ width = 50 mm)			
Welds A			
Without residual stresses	144.48	Ref.	0.292
With residual stresses	141.20	−2.27	0.280
Welds B			
Without residual stresses	161.47	Ref.	0.296
With residual stresses	164.77	2.05.	0.280
Welds A + Weld C1			
Without residual stresses	125.81	Ref.	0.259
With residual stresses	125.42	−0.31	0.228
Welds A + Weld C2			
Without residual stresses	132.25	Ref.	0.244
With residual stresses	128.92	−2.52	0.234
Welds B + Weld C1			
Without residual stresses	141.27	Ref.	0.246
With residual stresses	148.94	5.43	0.258
Plate of 7 mm			
Welds A			
Without residual stresses	180.12	Ref.	0.288
With residual stresses	171.57	−4.75	0.259

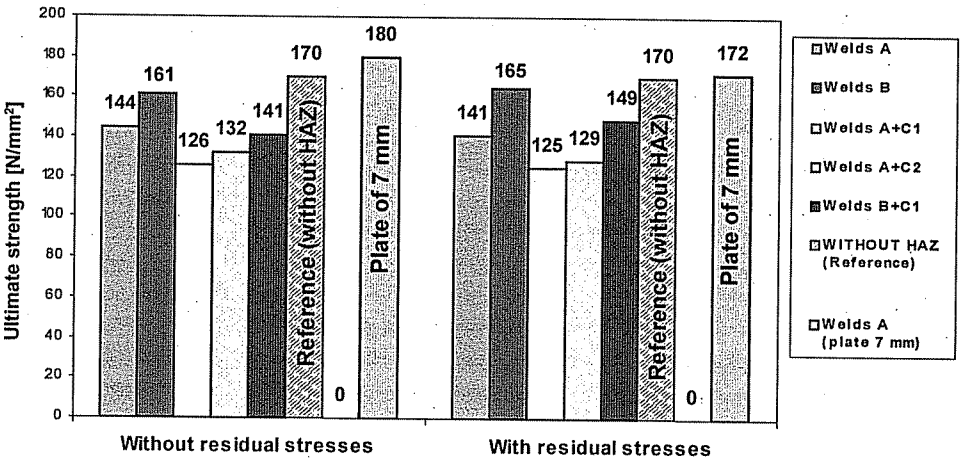

Fig. 22. *Phase B4*—sensitivity on residual stresses.

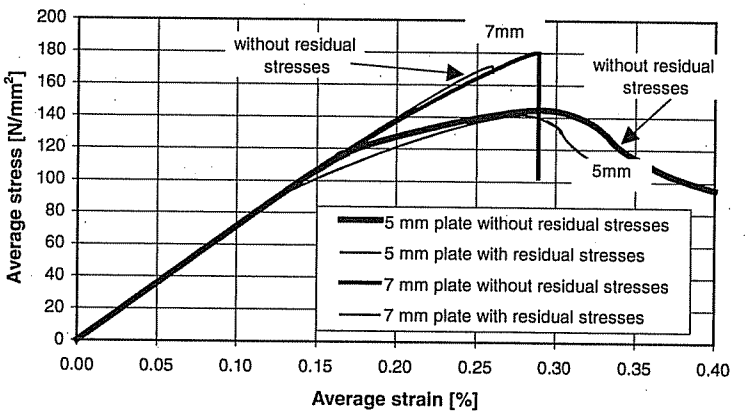

Fig. 23. Thickness effect for Welds A (*Phase B5*).

to 7 mm, keeping the rest of the geometry unchanged. The material properties and residual stresses correspond to Welds A, where the width of the HAZ is $2\eta_1 = 50$ mm. The ultimate strength curves in Fig. 23 show the behaviour with and without residual stresses for the two cases, 5 and 7 mm. The maximum average stress is presented in Table 7 (absolute and relative values are given).

According to Table 7 and Fig. 24, the ultimate strength of the considered stiffened panel increases by 11–12% due to an increase of 20% in plate thickness (i.e. 5–6 mm). This is an important conclusion with regards to the thickness uncertainty due to corrosion. It confirms that the plate thickness is one of the most sensitive parameter related to ultimate strength. Its influence depends also on the thickness range. In general, the compressive strength is very sensitive to plate thickness in a certain range of the panel slenderness.

Table 7
Phase B5: sensitivity on plate thickness—Welds A, 3 × 1025 mm spans model

	Maximum average stress		Average strain (%)
	(N/mm^2)	Difference to reference (%)	
Without residual stresses			
Plate thickness 5 mm	144.48	Ref.	0.292
Plate thickness 7 mm	180.12	24.6	0.288
With residual stresses			
Plate thickness 5 mm	141.20	Ref.	0.280
Plate thickness 7 mm	171.57	21.51	0.259

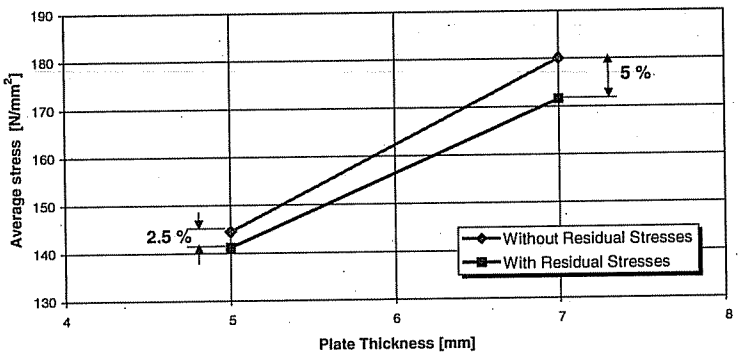

Fig. 24. Sensitivity on plate thickness (*Phase B5*).

4.8. *Phase B6—yield stress in the HAZ*

Analyses were done to assess the effect of the variation of yield stress in the HAZ on the ultimate strength. Plate and stiffener material properties and yield stress outside of the HAZ do not change. These analyses concern the configuration with Welds A (model with three spans 1025 mm) and with HAZ effect.

The initial material stress–strain curve in the HAZ (Fig. 2) is defined as "Sy(ref HAZ)". The modified curves considered to assess the effect of the yield stress in the HAZ are shown in Fig. 25. They are "Sy(ref HAZ)-10" up to "Sy(ref HAZ) + 60", with increments in N/mm^2.

The ultimate strength and the average stress–average strain curves are respectively presented in Table 8 and Fig. 26. According to Table 8, the ultimate strength does not vary linearly with the yield stress in the HAZ but almost linearly with its square root. So, the strength reduction due to yield stress variation may be assessed through the plate and column slenderness ratios of the panel that vary as the square root of the yield stress.

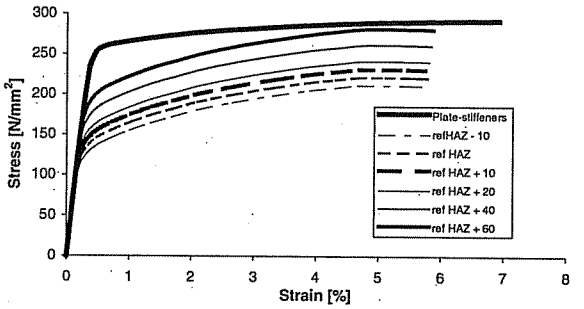

Fig. 25. Modified material stress–strain curves in the HAZ (*Phase B6*).

Table 8
Phase B6: sensitivity on yield stress of the HAZ, Welds A, 3 × 1025 mm spans model

Yield stress Philippe–Radu (shape 1)	Difference to reference		Maximum average stress		Average strain (%)
	Yield stress ratio (%)	Square root of yield stress ratio[a] (%)	(N/mm^2)	Difference to reference (%)	
Without HAZ			171.919		0.320
With HAZ—Welds A					
Sy (ref HAZ) −10	−7.7	−3.9	148.37	−1.31	0.313
Sy (ref HAZ)	0.00	0.00	150.34	0.00	0.311
Sy (ref HAZ) + 10	7.7	3.8	152.38	1.36	0.317
Sy (ref HAZ) + 20	15.4	7.4	154.35	2.67	0.317
Sy (ref HAZ) + 40	30.8	14.4	159.98	6.41	0.320
Sy (ref HAZ) + 60	46.2	20.9	167.70	11.55	0.307

[a] Varies as the column slenderness and the plate slenderness.

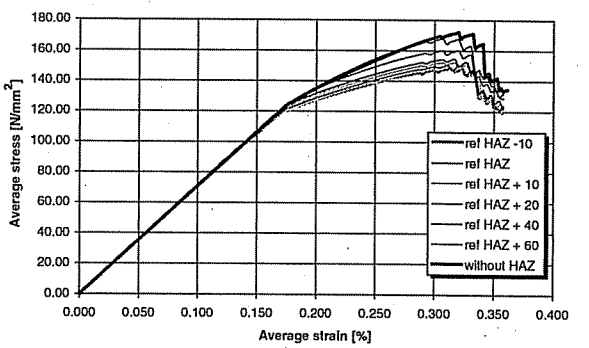

Fig. 26. Sensitivity of yield stress in the HAZ on the ultimate strength (*Phase B6*).

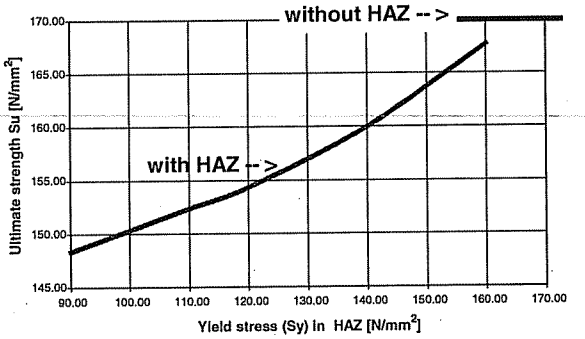

Fig. 27. Variation of ultimate strength versus yield stress in the HAZ (*Phase B6*).

Fig. 27 shows that a reduction of yield stress in the HAZ of 10% induces an ultimate strength reduction varying from 5% to 2%. The first reduction of yield stress has larger effect than additional reductions.

5. Other analyses

5.1. Explicit dynamic analysis

Fig. 28 compares the results of implicit FEM analyses with the results of an explicit analysis using a total loading time of 0.1 s. It is seen that the agreement between explicit and implicit analyses is very good.

Fig. 29 shows the stress–strain curves for two different loading times (0.1 and 0.01 s). It is clear that the effect of loading time is quite significant as the ultimate strength is increased by more than 30% when the loading time is reduced by a ratio of 10.

The large effect of loading time is caused by inertia loads, which become increasingly important as the loading rate increases. The difference between the two modes is quite evident: the quasi-statically loaded model deflected downwards in the central panel and the two outer panels deflected upwards while the panel loaded more dynamically failed in a mode where all three panels deflected upwards, as prescribed by the initial deflections.

In conclusion, any explicit analysis of a quasi-static problem requires a very careful consideration and extensive parameter studies of the loading rate in order to assure that non-physical dynamic effects are not dominating the solution.

5.2. Convergence assessment

Additional analyses with HAZ effects (*Phase A* and Welds A) were completed by Wan using about 20 different FE meshes that include, respectively, 1866, 4242, 6042, 7150, 7842, 9642 and 12292 shell elements (Tables 1 and 9; Figs. 30 and 31). The results show that the convergence of the ultimate stress is quite good. However, the

Contributors (Shape 1)	s_u [N/mm^2]
Philippe-Radu	171.92
Lehmann-Catalin	169.88
Yao-Higashiyama	160.80
Bo-Ulrik	168.00
Explicit Model	

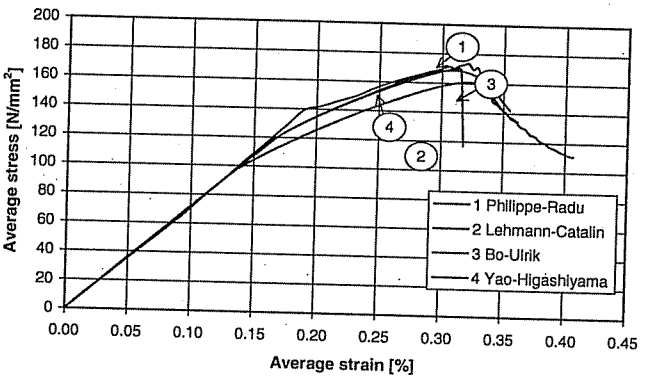

Fig. 28. Implicit analysis versus explicit dynamic analysis (without HAZ)—with a total loading time of 0.1 s.

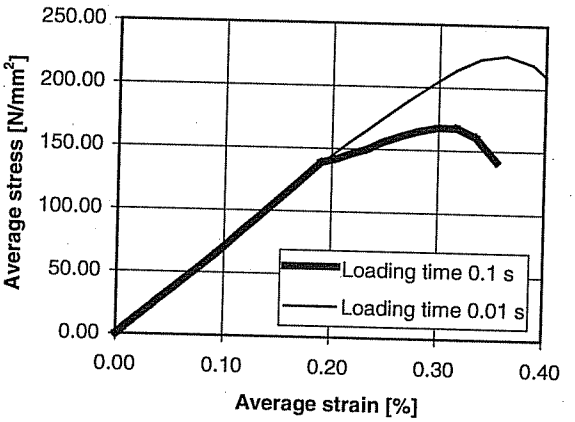

Fig. 29. Explicit analysis with two different loading times.

Table 9
Convergence analysis—Welds A, 3 × 1025 mm spans model

Number of elements	1866	4242	6042	7150	7842	9642	11292
Ultimate stress (N/mm^2)	137.99	107.96	102.37	100.02	99.44	99.35	99.19

convergence rate slows down when the number of elements increases. For the present collapse analysis of stiffened aluminium panels, the optimal mesh size seems to require about 8000 elements (Tables 1 and 9). It seems that an 8000 elements model including 5×10 or 5×12 elements in the "Y" transverse direction and 3×40 elements in the "X" longitudinal direction is convenient to determine the maximum average stress (ultimate strength). However, if the post-ultimate strength has to be considered, at least 5×16 elements in "Y" direction and 3×50 elements in "X" direction are needed (about 12,000 elements).

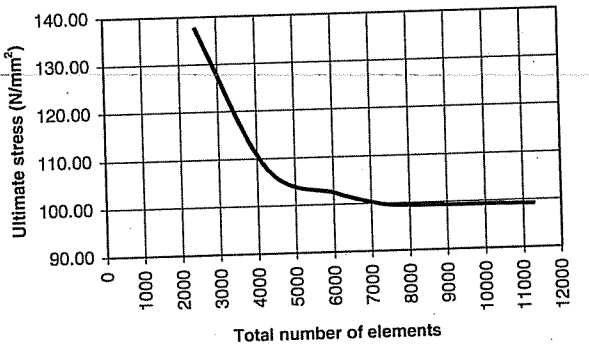

Fig. 30. Sensitivity of the mesh size (convergence assessment).

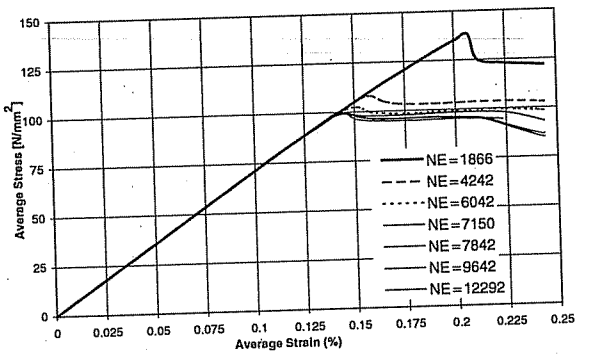

Fig. 31. Effect of the mesh size on the analysis: Convergence assessment (*Phase A*, with HAZ, Welds A).

6. Conclusions

The aim of this study was to validate a non-linear finite element model for calculation of the ultimate compressive strength of stiffened aluminium panels. Consequently, a calibration assessment was done comparing the results of contributors that performed an identical analysis with different codes.

Then, contributors carried-out finite element analyses to assess the sensitivity on the ultimate strength of welding join types, HAZ width, initial panel deflection (amplitude and shape), residual stress, plate thickness and yield stress in the HAZ. Numerical simulations have shown that the plastic buckling analyses of the considered aluminium stiffened panel, which are based on the incremental theory of plasticity, are significantly sensitive to these parameters.

The results from *Phase A* have led to the choice of a new and more appropriate geometry to achieve the sensitivity analyses (*Phase B*). *Phase A* (three spans of 2050 mm) shows that HAZ has no significant effect for a slender panel with low ultimate strength but as the panel becomes stockier and thus experiences plastic buckling, the sensitivity becomes more important.

In *Phase B* (three spans of 1025 mm), the sensitivity analysis have provided quantitative assessments (only valid for the considered structures):

6.1. Welds types (HAZ effect)

- The reduction of ultimate strength varies from 0% to 30%.
- Configuration with Welds B (extruded elements) is less sensitive to HAZ than with Welds A (stiffeners welded on the plate), respectively, 13–17% and 1–6%.
- Most sensitive configuration concerns configuration with welded stiffeners (Welds A) and one transverse weld (Weld C1 or Weld C2): 23–27%.
- A single transverse weld (C1 or C2) may induce a reduction of about 11–12%.

6.2. HAZ width

The variation of ultimate strength is not proportional to the HAZ width. The reduction induced by the first 25 mm of HAZ width ($2\eta_1 = 25$ mm) is twice the additional reduction induced by another 25 mm of HAZ width.

For a standard width ($2\eta_1 = 50$ mm in plate and $\eta_2 = 25$ mm in stiffener web), the ultimate strength reduction is about 4%.

6.3. Initial imperfection

About 1% of reduction is recorded for each mm of initial deflection at mid-span of the central stiffener.

6.4. Residual stresses

The strength reduction induced by the residual stresses is about −2.5% (plate 5 mm thick). This variation depends significantly on the weld types, for instance from a reduction of −5% to an increase of strength of +2% (Welds B for extruded elements). Such increase has to be confirmed by more advanced analyses and experiments. Effect of residual stresses with a plate 7 mm thick is twice the effect with a plate of 5 mm.

6.5. Yield stress in the HAZ

A reduction of yield stress in the HAZ of 10% induces an ultimate strength reduction varying from 5% to 2%. The first reduction of yield stress has lager effect than additional reductions.

6.6. Explicit analysis

An explicit analysis can be performed as an alternative to standard implicit FEA. It requires a very careful consideration and extensive parameter studies of the

loading rate to assure that non-physical dynamic effects are not dominating the solution.

6.7. Convergence

Coarse meshes (1000–5000 elements) are not suitable to study collapse analysis of stiffened aluminium panels. For the concerned model, an optimal mesh size seems to require about 8000 elements to get the ultimate strength and about 12,000 elements to assess the post collapse behaviour.

In the future, this sensitivity assessment has to be continued with the study of other parameters and panel configurations. The present results could be completed by a comparison with rules, codes (Eurocode 9) and experimental results given by the literature. The effect of the aluminium material property modelling (stress–strain relation) on the ultimate strength has also been studied in the near future to develop closed-form design formulations.

Acknowledgements

The authors thank Mr. U. Borg, student at the Technical University of Denmark, for his contribution.

References

[1] Aalberg A, Langseth M, Larsen PK. Stiffened aluminium panels subjected to axial compression. Thin Walled Struct 2001;39:861–85.
[2] Aalberg A, Langseth M, Malo KA. Ultimate strength of stiffened aluminium plates. Norwegian University of Science and Technology, Department of Structural Engineering, 1998.
[3] Kristensen QHH, Moan T. Ultimate strength of aluminium plates under biaxial loading. In: Proceedings of the Fifth International Conference on Fast Sea Transportation, New York, 1999.
[4] Zha Y, Moan T, Hanken E. Experimental and numerical study of torsional buckling of stiffeners in aluminium panels. In: Proceedings of the Fifth International Conference on ISOPE, Seattle, May 2000. p. 249–55.
[5] Zha Y, Moan T, Hanken E. Ultimate strength of stiffened aluminium panels with predominantly torsional failure modes. Thin-Walled Struct 2001;39:631–48.
[6] Zha Y, Moan T. Experimental and numerical prediction of collapse of flatbar stiffeners in aluminium panels. J Struct Eng 2003;129(2):160–8.
[7] Hopperstad OS, Langseth M, Hanssen L. Ultimate compressive strength of plate elements in aluminium: correlation of finite element analyses and tests. Thin-Walled Struct 1998;29:31–46.